Dramatic Slowdown of Bimolecular Reactions of Criegee Intermediates in Organic Aerosols

Meirong Zeng [a] and Kevin R. Wilson [b]**

[a] *College of Smart Energy, Shanghai Jiao Tong University, Shanghai 200240, P.R. China*

[b] *Chemical Sciences Division, Lawrence Berkeley National Laboratory, Berkeley, California 94720, United States.*

*** Corresponding Authors:** *Meirong Zeng (email: meirongzeng@sjtu.edu.cn) and Kevin R. Wilson (email: krwilson@lbl.gov)*

Abstract

Although Criegee intermediates (CIs) play a central role in driving the transformation of organic molecules, their condensed-phase reaction kinetics remain poorly understood. While CIs undergo unimolecular decomposition to produce OH radicals, stabilized CIs participate in a host of other bimolecular reactions forming larger molecular weight products, including secondary ozonides (k_{SOZ}), alkoxyalkyl hydroperoxides (k_{AlAHP}), and acyloxyalkyl hydroperoxides (k_{AcAHP}). Here we demonstrate, using prior literature and new measurements of heterogeneous organic aerosol reactions using O_3 or OH radicals, that these condensed-phase bimolecular reaction rate coefficients k_{SOZ} (10^{-20} $cm^3 \cdot molecule^{-1} \cdot s^{-1}$), k_{AlAHP}, and k_{AcAHP} (10^{-19} $cm^3 \cdot molecule^{-1} \cdot s^{-1}$) are 7-10 orders of magnitude slower than analogous gas-phase reactions (~ 10^{-10} - 10^{-13} $cm^3 \cdot molecule^{-1} \cdot s^{-1}$). This contrasts with current evidence that the rate coefficients for unimolecular steps in the condensed phase are similar in magnitude to those in the gas phase. Kinetic models using gas-phase-like bimolecular coefficients consistently overestimate the importance of bimolecular relative to unimolecular pathways while underpredicting the aerosol reactivity by up to 30-fold. The slowing of bimolecular reactivity in aerosols is likely due to solvation effects and the increased steric hindrance of larger molecular weight CIs and their scavengers in the condensed phase. These results challenge the conventional view that the high reactant density of an organic aerosol should favor bimolecular over unimolecular reactions; underscoring the need for more accurate CI condensed-phase rate constants for reliable modeling of oxidative processes across diverse set of atmospheric and environmental systems.

Keywords

Criegee intermediates, organic aerosols, heterogeneous oxidation, dramatic slowdown rates

Synopsis

Bimolecular reactions of Criegee intermediates in aerosols (forming secondary ozonides and hydroperoxides) proceed at 7-10 orders of magnitude slower than in gas phase, leading to an underestimate of OH-driven autoxidation rates in organic aerosols by 30-fold.

1. Introduction

Criegee intermediates (CIs), highly reactive carbonyl oxides, are key intermediates in the oxidation of organics formed through reactions with ozone (O_3) and hydroxyl radicals (OH) in atmospheric, environmental, and biological systems.[1-3] First characterized by Rudolf Criegee,[1] these intermediates form via cycloaddition of O_3 to carbon-carbon double bonds of unsaturated hydrocarbons, yielding primary ozonides (POZs) illustrated in Fig. 1. POZ decomposition generates CIs with carbonyl co-products. Recent studies[4-8] reveal an alternative radical mediated formation pathway where OH initiated oxidation of unsaturated hydrocarbons produces β-hydroxy peroxy radicals (β-OH-$RO_2^{\bullet}$) whose subsequent reaction steps appear to lead to a non-ozonolysis source of CIs. Beauchamp and coworkers[4] provided the first experimental evidence for CI formation from β-OH-$RO_2^{\bullet}$ during the reactions of lipid droplets with OH radicals. Wilson and coworkers[6-8] later demonstrated that this process plays a dominant role in driving lipid autoxidation (Fig. 1). Despite these advances, the detailed mechanism of how β-OH-$RO_2^{\bullet}$ decomposition into CIs remains unsolved and further theoretical investigation is needed. [8-10]

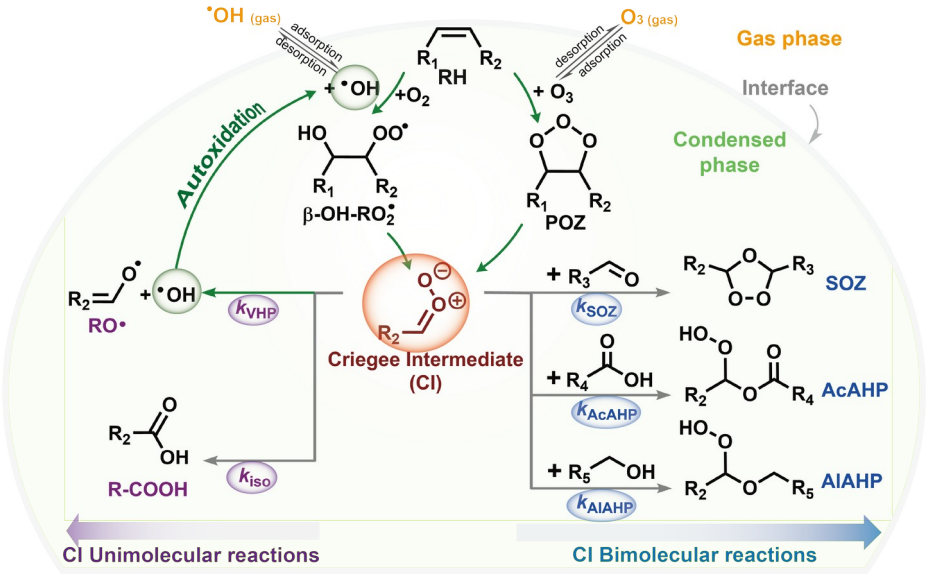

Figure 1. Heterogeneous oxidation mechanism of unsaturated aerosols (RH) initiated by gas-phase O_3 or OH radicals, illustrating formation pathways of Criegee Intermediates (CI) and subsequent consumption reactions: unimolecular decomposition via vinyl hydroperoxide formation (k_{VHP}) and isomerization (k_{iso}); bimolecular reactions with aldehyde forming secondary ozonide (k_{SOZ}), carboxylic acid producing acyloxyalkyl hydroperoxide (k_{AcAHP}), and alcohol generating alkoxyalkyl hydroperoxide (k_{AlAHP}).

The decomposition pathways of CIs govern the budgets of key species, particularly OH radicals, acids, alcohols, aldehydes, hydroperoxides (ROOH), and secondary organic aerosol (SOA) [11]. The fate of CIs is predominantly determined by their internal energy distribution. For example, chemically activated CIs, with internal excitation undergo rapid unimolecular reactions [3, 12]. A representative pathway involves 1,4-hydrogen migration to yield a vinyl hydroperoxide (VHP) intermediate (Fig. 1), which subsequently dissociates into an OH and vinoxy radical [13]. In contrast, stabilized (*i.e.*, thermalized) CIs react via bimolecular pathways with aldehydes, carboxylic acids, and alcohols, forming more complex molecules such as secondary ozonides (SOZ), acyloxyalkyl hydroperoxides (AcAHP), and alkoxyalkyl hydroperoxides (AlAHP). The atmospheric consequences of these pathways are distinct: unimolecular decomposition reduces

carbon chain length and generates OH radicals, serving as a non-photolytic source of atmospheric OH, thereby sustaining autoxidation chain reactions [6, 14]. Alternatively, CI bimolecular reactions with aldehydes, alcohols, or carboxylic acids form higher molecular weight functionalized products (e.g., SOZ, AlAHP, and AcAHP), ultimately affecting SOA formation and growth dynamics [15].

Decades of experimental and theoretical work have yielded well-constrained gas-phase rate constants for CI decomposition [12, 16-21], with example values shown in Fig. 2 and Table S1. Taatjes *et al.* [20] directly measured the bimolecular rate constant of the simplest CI (CH_2OO) with acetaldehyde by laser photolysis/tunable synchrotron photoionization mass spectrometry, reporting a value of 9.5×10^{-13} $cm^3 \cdot molecule^{-1} \cdot s^{-1}$. Chao *et al.* [21] computed a rate constant of 4.8×10^{-12} $cm^3 \cdot molecule^{-1} \cdot s^{-1}$ for the reaction of a C_2-CI with methanol. Welz *et al.* [22] and Khan *et al.* [23] showed that C_1 to C_3 CIs react with formic and acetic acid at near a collision limited rate (*i.e.*, 10^{-10} $cm^3 \cdot molecule^{-1} \cdot s^{-1}$). Tobias *et al.*[24] determined the gas-phase rate constants for a larger C_{13} CI with 2-propanol (10^{-13} $cm^3 \cdot molecule^{-1} \cdot s^{-1}$), formaldehyde ($10^{-11}$ $cm^3 \cdot molecule^{-1} \cdot s^{-1}$), and heptanoic acid ($10^{-10}$ $cm^3 \cdot molecule^{-1} \cdot s^{-1}$) using real-time quantitative thermal desorption particle beam mass spectrometry. Consistent rate constants for reactions of C_1 CI with C_1-C_6 alcohols have also been reported Wang *et al.*[25] and reactions of C_1 CI with butyraldehydes have been demonstrated by Debnath *et al.*[26] Chhantyal-Pun *et al.*[27] developed a structure-activity relationship (SAR), reporting consistent rate constants (10^{-10} $cm^3 \cdot molecule^{-1} \cdot s^{-1}$) for reactions of C_1-C_{10} CIs (*syn* or *trans*) with C_1-C_{10} acids. Specifically, these C_1-C_{10} CIs include the simplest CH_2OO, syn-CH_3CHOO, anti-CH_3CHOO, syn-pinonaldehyde oxide (C_{10} CI), and anti-pinonaldehyde (C_{10} CI).[27] In contrast, Watson *et al.*[28] observed a significant conformational dependence for the reactions of CH_3CHOO

with methanol, with rate constants differing by several orders of magnitude between the *syn*- (10^{-17} $cm^3 \cdot molecule^{-1} \cdot s^{-1}$) and *anti*- ($10^{-12}$ $cm^3 \cdot molecule^{-1} \cdot s^{-1}$) conformers. This marked difference indicates that bimolecular reactions with alcohols are highly sensitive to the specific conformers of the CI,[28] unlike reactions with acids, where conformational effects are relatively small.[27] In the absence of condensed phase measurements, these gas-phase rate constants are often used to condensed-phase kinetic models to evaluate the role of CI in governing the transformation of organic molecules [29].

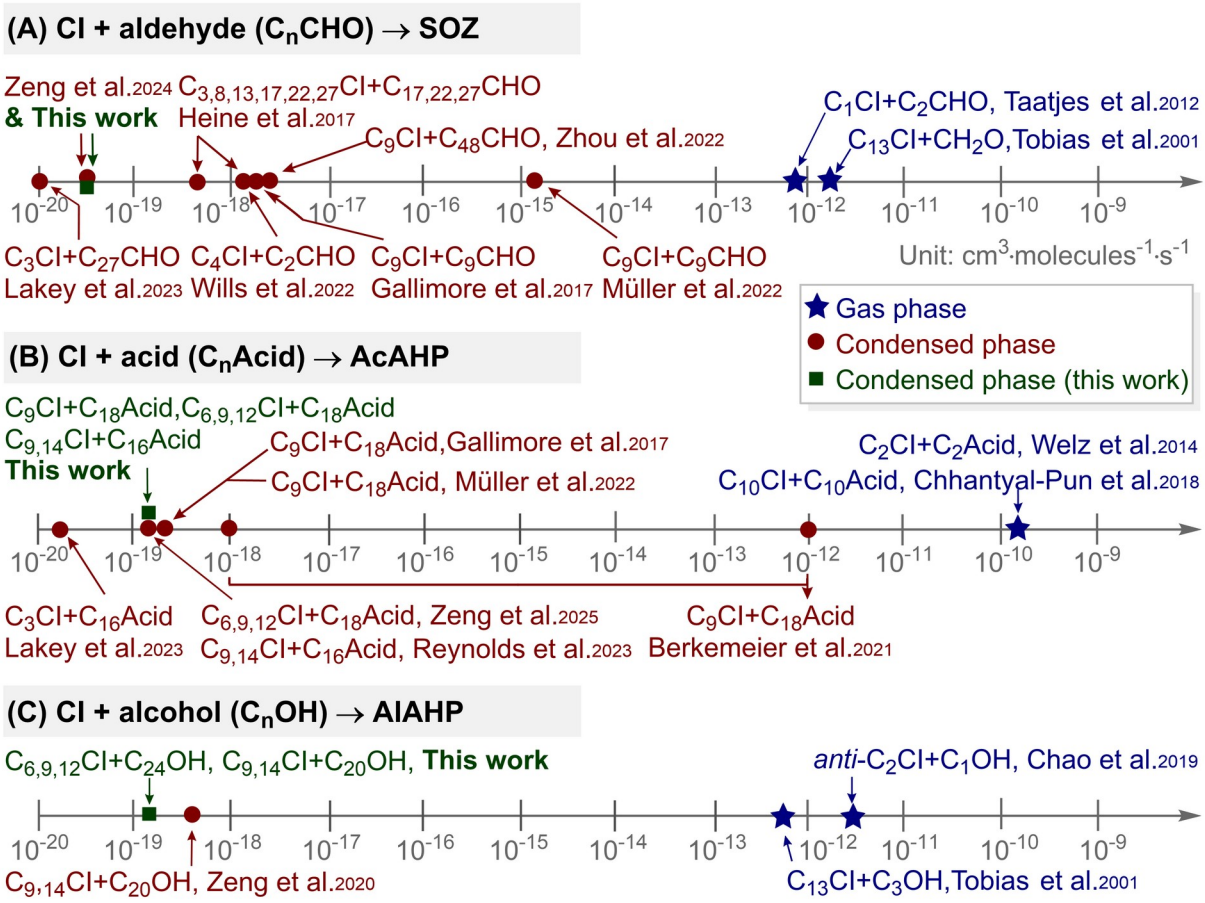

Figure 2. Comparative analysis of Criegee intermediate (CI) rate constants for (A) CI + aldehyde (C_nCHO) forming secondary ozonide (k_{SOZ}), (B) CI + carboxylic acid (C_nAcid) yielding acyloxyalkyl hydroperoxide (k_{AcAHP}), and (C) CI + alcohol (C_nOH) producing alkoxyalkyl hydroperoxide (k_{AlAHP}). Abbreviated chemical compositions of representative CIs and scavengers are provided. The comparison includes literature-reported gas-phase [20-22, 24, 27] and condensed-phase values [7, 8, 14, 30-37], some of which are from our previous work.[7, 8, 14, 35-37]

Recent evidence suggests that condensed phase CIs react with aldehydes (k_{SOZ}), alcohols (k_{AlAHP}), and carboxylic acids (k_{AlAHP}) with much smaller rate constants (i.e., $< 10^{-17}$ cm$^3 \cdot$ molecule$^{-1} \cdot$ s^{-1}) albeit with a large range of uncertainty (10^{-12}-10^{-20} cm$^3 \cdot$ molecule$^{-1} \cdot$ s^{-1} as illustrated in Fig. 2 and Table S2 [7, 8, 14, 30-37]). Relative to the gas phase these condensed phase rates are up to ten orders of magnitude slower than analogous gas-phase reactions involving small CIs [6-8]. This dramatic rate slowdown appears in heterogeneous reactions involving organic particles exposed to both gaseous O_3 or OH radicals, as reported in our previous work.[7, 8, 14, 35-37] For example, studies of aerosols comprised of squalene ($C_{30}H_{50}$, denoted Sqe) and cis-9-tricosene ($C_{23}H_{46}$, Tri) reveal that CI reactions with aldehydes, carboxylic acids, and alcohols proceed with bimolecular rate constants (k_{SOZ}, k_{AlAHP} and k_{AlAHP}) between 10^{-20} to 10^{-18} cm$^3 \cdot$ molecule$^{-1} \cdot$ s^{-1}. Notably, Müller *et al.* [32] reported a larger value for k_{SOZ} (10^{-15} cm$^3 \cdot$ molecule$^{-1} \cdot$ s^{-1}) obtained from the ozonolysis of oleic acid ($C_{18}H_{34}O_2$, OA) aerosols, based on a kinetic model fit to their experimental data. This slowdown, due to phase, appears to affect mainly bimolecular pathways, since modeling evidence to date shows that unimolecular decomposition rates of CI remain similar to those measured in the gas phase (Table S2). For example, the CI unimolecular reaction generating OH radicals ($k_{VHP} = 10^2$ s^{-1}) [6-8]. Besides, the reactivity of CIs is highly sensitive to their molecular structure and conformation,[12, 28] with rate constants differing by orders of magnitude. These observations raise questions as to whether the main reactive sink for CIs in aerosols are either bimolecular or unimolecular and whether these sinks differ significantly from those predicted for the gas phase. Given that the present study employs representative rate coefficients (e.g., k_{SOZ}, k_{AlAHP} and k_{AlAHP}) for condensed-phase CIs, the development of structure-specific reactivity parameters for long-chain condensed-phase CIs remains a goal for future theoretical and modeling studies.

This study investigates heterogeneous oxidation of organic aerosols using two approaches: O_3 initiated CI reactions in a flowtube reactor (Fig. S1), and OH initiated CI reactions in a continuous flow stirred tank reactor (Fig. S2), see the *Materials and Methods*. Real-time kinetics and product analysis are performed using a vacuum ultraviolet aerosol mass spectrometer (VUV-AMS) [38, 39]. We quantify the effective reaction probability (γ_{eff}) [40], defined as the fraction of oxidant (O_3 or OH) collisions that result in an aerosol reaction. For reactions of OH radicals with organic aerosols, $\gamma_{eff} \leq 1$ corresponds to reactions that occur at or below the gas-particle collision limit. Values of γ_{eff} exceeding 1 provide evidence for radical chain propagation reactions (*e.g.,* autoxidation) where a single reactive collision initiates multistep reactions [6, 40]. To quantitatively constrain CI bimolecular reaction rates, we developed kinetic models implemented in either *Kinetiscope* [41, 42] or *Mathematica* [43] (see *Materials and Methods*). These models use established literature mechanisms and rate coefficients where applicable. Together, these experimental and modeling approaches are used to further constrain CI bimolecular reaction rates that establish CIs reactions as rate-limiting steps in aerosol oxidation [6].

2. Materials and Methods

2.1. Experimental Setup

Two complementary multiphase reactors are employed to study the heterogeneous oxidation of organic aerosols: a flowtube reactor for O_3 oxidation (Fig. S1) and a continuous flow stirred tank reactor (CFSTR) (Fig. S2) for OH-initiated oxidation [44]. Chemistry in both reactors is conducted at atmospheric pressure and room temperature. Additional experimental details are provided in supporting information. Polydisperse organic aerosols were generated via the homogeneous nucleation by passing dry N_2 through a heated Pyrex tube containing liquid samples of the

unsaturated organics (with or without saturated CI scavengers). Furnace temperatures are optimized for each experiment based on the vapor pressures of organics [6]. Upon cooling the flow nucleation occurs and particles form in log-normal distribution (~ 10^6 cm^{-3}, diameter ~ 200 nm), characterized using a scanning mobility particle sizer (SMPS, TSI 3080L DMA and 3025A CPC). The aerosol is passed through an annular activated charcoal denuder to remove any residual gas-phase contributions to the aerosols, yielding a final aerosols concentration in the reactors of ~ 2000 $\mu g/m^3$. Prior to entering the reactors, the aerosol flow was mixed with oxidants (H_2O_2 or O_3), dry N_2, and O_2.

For O_3 oxidation experiments, the aerosol-gas mixture is introduced into a flowtube reactor (140 cm long and 2.5 cm inner diameter) with an average residence time of ~37 s at a total flow of 1.1 SLM. O_3 is produced by passing 0.05 SLM O_2 through a corona-discharge generator, followed by dilution with dry N_2 (3 SLM) to achieve adjustable O_3 concentrations (0-10 ppm) that are monitored using an ozone analyzer (2B technology Model 202M). For OH oxidation experiments in the CFSTR, OH radicals are generated *in-situ* by photolyzing gas-phase H_2O_2 using two 45 cm UV lamps (blacklights, λ ~ 356 nm), which are housed within 2.54 cm diameter GE type 214 quartz sleeves. [OH] is controlled by adjusting the UV lamp power. Gaseous H_2O_2 (< 10 ppm in CFSTR) is produced by passing 0.1 SLM N_2 through a heated bubbler (60 °C) containing a 1:1 mixture of urea-hydroperoxide ($CO(NH_2)_2 \cdot H_2O_2$, Sigma-Aldrich, 97% pure) and sand (50-Silicaa 70 mech particle size, Sigma-Aldrich). An additional flow containing gas-phase tracer (2-methyl-2-butene, ~ 200 ppb), monitored by a gas chromatograph with a flame ionization detector (GC-FID, SRI Instruments 8610C), is used to quantify [OH] via relative rate technique [44]. Control

experiments confirm tracer presence did not alter the overall chemistry. The CFSTR experiments operate at ~ 1.1 SLM total flow, enabling reaction timescales up to hours.

Aerosol chemical compositions were analyzed using a custom-built vacuum ultraviolet aerosol mass spectrometer (VUV-AMS) [38, 39] at the Chemical Dynamics Beamline (9.0.2) of the Advanced Light Source (Lawrence Berkeley National Laboratory, LBNL). In AMS, aerosol samples were vaporized at ~130 ºC and subsequently photoionized with the VUV light filtered by an argon gas filter and a MgF_2 window to remove undulator harmonics. Variable photon energies were used for each experiment to minimize fragmentation (e.g., 9.6 eV for Sqe, and 10.2 eV for LA/OA). Product abundances are scaled to simulated concentrations from the Base model due to the challenges in absolute quantification arising from uncharacterized photoionization cross-sections and ion fragmentation probabilities [6-8, 14].

2.2. Kinetic Simulation Methods

The heterogeneous reaction kinetics of organic aerosols exposed to gas-phase O_3 or OH radicals are simulated using Kinetiscope© [41, 42]. Organic aerosols are modeled as a single instantaneously mixed compartment with dimensions 1 nm × 1 nm × (R/3) nm (R = experimentally measured radius of the aerosols), to represent surface-to-volume scaling for spherical aerosols. Heterogeneous oxidation is described by three main steps: (i) adsorption of gas-phase O_3 or OH radicals onto the aerosol surfaces forming surface-absorbed O_3 or OH radicals; (ii) condensed-phase reactions of organic aerosols initiated by adsorbed O_3 or OH radicals; and (iii) evaporation of volatile products. Steps (i) and (iii) have been described previously [37, 42, 45-47]. Extending established base models for Tri + $C_{20}OH$ + O_3 [14], Tri + HDA + O_3 [35], Sqe + OH [8] systems,

we developed test models implementing faster k_{AlAHP}, k_{AcAHP}, and k_{SOZ} (10^{-13} $cm^{-3} \cdot molecule^{-1} \cdot s^{-1}$), approximating gas-phase values [23]) as detailed in Table S4.

Additional analytical models implemented in *Mathematica*© (see supporting text and Table S5) were developed for reaction systems lacking established explicit Kinetiscope models. These include OA (LA) + O_3, OA (LA) + $C_{24}OH$ + O_3, and Tri (OA or LA) + $C_{24}OH$ + OH reactions. These analytical models explicitly focus on dominant reaction pathways while omitting adsorption and evaporation dynamics included in the Kinetiscope framework. These more simplified analytical models capture essential CI chemistry through two principal pathways: CI formation via O_3 or OH radical oxidation of Tri, OA, and LA and CI consumption through unimolecular decomposition and bimolecular reactions with scavengers ($C_{24}OH$, OA, and LA). This framework retains predictive capability for key kinetic parameters, including reactants and characteristic products. Validation of these more simple approaches comes from Reynolds *et al.* [35], who demonstrated quantitative consistency between analytical and Kinetiscope models in determining bimolecular reaction rates for CIs + HDA reactions (k_{AcAHP}) during the ozonolysis of Tri + HDA aerosols.

3. Results and Discussion

We designed an experimental framework by integrating present measurements with reference data (Table S3) to quantify the bimolecular reaction rates of CIs: k_{SOZ}, k_{AcAHP}, and k_{AlAHP}. We examine four unsaturated organic aerosols: Sqe, Tri, linoleic acid ($C_{18}H_{32}O_2$, LA), and oleic acid ($C_{18}H_{34}O_2$, OA), together with three saturated CI scavengers: 2-octyl-1-dodecanol ($C_{20}H_{42}O$, $C_{20}OH$), 2-decyl-1-tetradecanol ($C_{24}H_{50}O$, $C_{24}OH$), and 2-hexyldecanoic acid ($C_{16}H_{32}O_2$, HDA). Sqe constitutes approximately 12% of human sebum [48], while LA and OA are major unsaturated

fatty acids in cell membranes [49, 50]. The saturated $C_{20}OH$, $C_{24}OH$ and HDA are simple models for alcohols and acids that act as CI sinks in atmospheric, environmental, and biological systems. The molecular diversity of these compounds (Fig. 3), spanning the number and kinds of C=C bonds and functional groups, enables controlled investigations of how chemical structures of organic aerosols influence CI formation rates and subsequent competitive consumption pathways. Three experimental approaches are used. For functionalized organic aerosols (LA or OA), as well as those generating condensed-phase aldehyde products during oxidation (Sqe), CIs undergo bimolecular reactions with these organics (including LA and OA) or aldehyde products. For non-functionalized organic aerosols (Tri), a saturated CI scavenger (e.g., HDA, $C_{20}OH$, and $C_{24}OH$) is added to the aerosol as a bimolecular sink. For functionalized organic aerosols with added CI scavengers, the rates of two competing bimolecular reactions of CIs can be constrained.

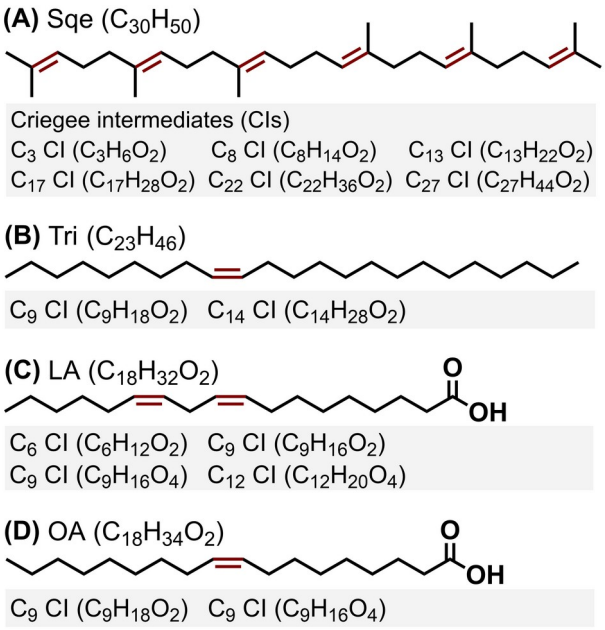

Figure 3. Chemical structures of Sqe, Tri, LA, and OA, and their corresponding Criegee intermediates (CIs) formed during heterogeneous oxidation.

Figure 4A shows prior evidence[14] demonstrating that $C_{20}OH$ serves as the dominant condense-phase bimolecular sink for CIs during the ozonolysis of Tri aerosols, producing AlAHPs. The reaction mechanism (Figs. S4 and S5) begins with O_3 addition to the single C=C bond of Tri, forming a POZ that decomposes to yield C_9 and C_{14} CIs along with two volatile aldehyde co-products. These aldehydes preferentially partition into the gas phase, which minimizes their participation as CI scavengers. By introducing saturated $C_{20}OH$ as a CI scavenger, CI formation is decoupled from bimolecular consumption pathways while enabling precise control over CI scavenger concentration, thereby allowing quantitative determination of k_{AlAHP} under controlled conditions.

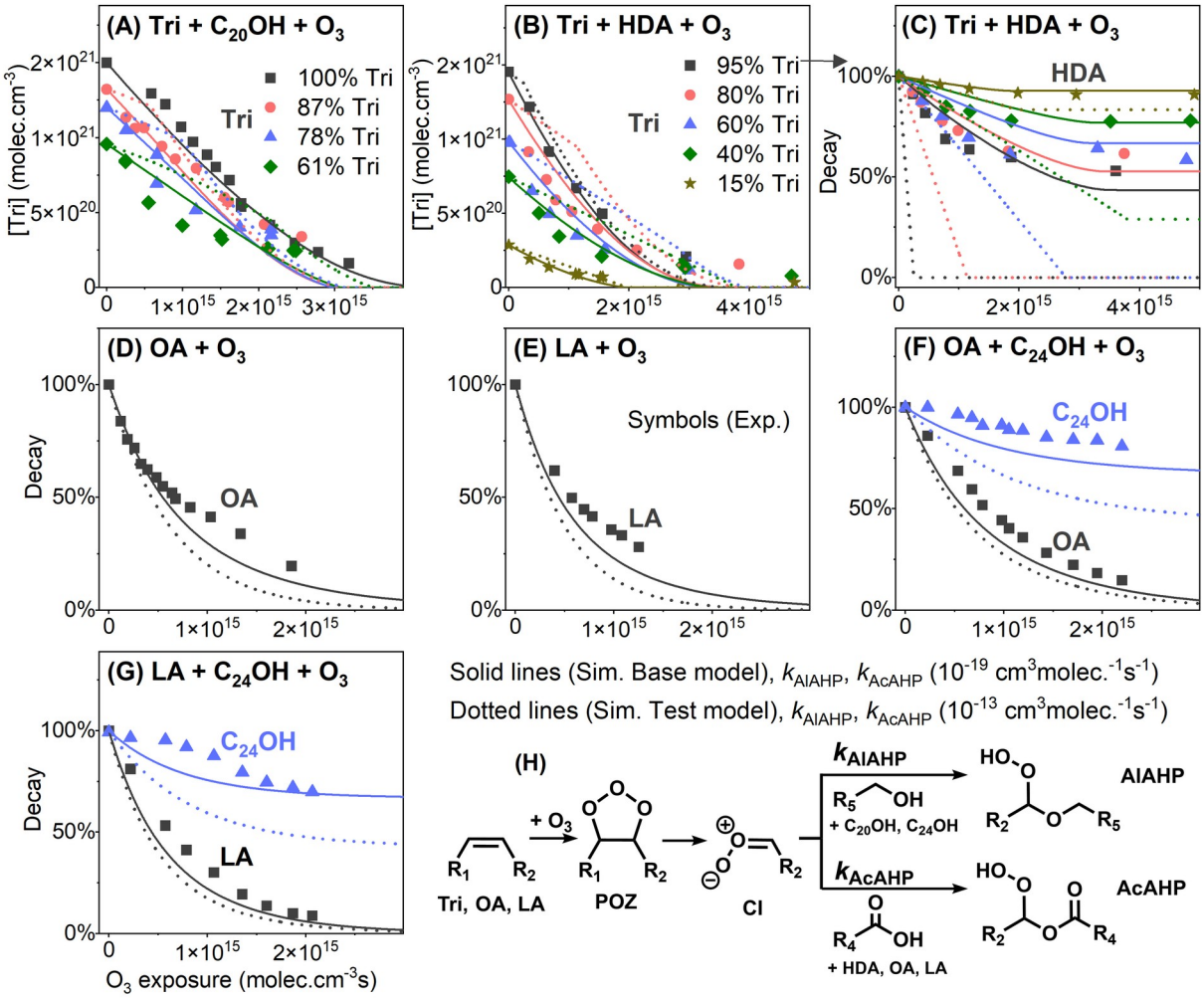

Figure 4. (A-G) Experimental kinetics (symbols) and model simulations (lines) for the ozonolysis systems containing Tri [14, 35], OA, and LA with or without external CI scavengers ($C_{20}OH$, $C_{24}OH$, and HDA) in the flowtube reactor. Solid and dotted lines represent simulations from the base model (incorporating condensed-phase rate constants) and test model (assuming gas-phase-equivalent rates), respectively. For example, panel A depicts the decay of Tri as a function of O_3 exposure for Tri + $C_{20}OH$ mixtures (100% Tri to 61% Tri + 39% $C_{20}OH$). Panels B and C show the decay of Tri and HDA, representatively, for Tri + HDA mixtures (with Tri content ranging from 95% to 15%). (H) Reaction scheme showing CI formation from ozonolysis of unsaturated organics (Tri, OA, and LA), followed by CI bimolecular reactions with alcohols ($C_{20}OH$ and $C_{24}OH$) or carboxylic acids (HDA, OA, and LA). Note that while the decomposition of a POZ can yield two CIs, only one representative structure is depicted in panel H.

To quantify k_{AlAHP}, we implemented an established kinetic mechanism (*see Materials and Methods*) [14] as a base model, using a rate constant $k_{AlAHP} = 6.7 \times 10^{-19}$ $cm^{-3} \cdot molecule^{-1} \cdot s^{-1}$. This base model replicates the experimental decay kinetics of Tri observed across varying concentrations of the CI scavenger ($C_{20}OH$). In contrast, a test model using a faster, gas-phase equivalent rate of $k_{AlAHP} = 10^{-13}$ $cm^{-3} \cdot molecule^{-1} \cdot s^{-1}$ [23] predicts a significantly slower decay of Tri, which deviates from the measured data. This kinetic discrepancy results from excessive scavenging by $C_{24}OH$ through bimolecular termination of CIs, which competitively inhibits the unimolecular decomposition of CIs that otherwise regenerate OH radicals. Consequently, this suppression reduces subsequent OH-initiated oxidative decay of Tri [14], as illustrated in Fig. 1. Consistent with this mechanism, the test model predict much earlier formation of AlAHPs as illustrated in Fig. S4B. In summary, the test model with gas-phase-like k_{AlAHP} underpredicts the oxidative transformation of unsaturated aerosols, while overpredicting the formation of high-molecular-weight products (AlAHPs); leading to significant discrepancies from the condensed-phase experimental observations.

Figures 4B and 4C show reference experimental data from Reynolds *et al.* [35] in which 2-hexyldecanoic acid (HDA) is the dominant sink for CIs during the ozonolysis of Tri. From this experiment it was determined that the condensed-phase bimolecular rate constant (k_{AcAHP}) for the CIs + HDA reaction is 2.2×10^{-19} $cm^{-3} \cdot molecule^{-1} \cdot s^{-1}$) (Figs. S6-S7). In contrast, a test model implementing a diffusion limited rate constant of $k_{AcAHP} = 10^{-13}$ $cm^{-3} \cdot molecule^{-1} \cdot s^{-1}$ predicts significantly slower Tri decay and faster HDA consumption that is observed in the experiment. Extending this framework to biologically relevant unsaturated fatty acids [49, 50], *i.e.*, oleic acid (OA) and linoleic acid (LA), we observe their dual functionality in ozonolysis reactions (Figs. 4D-4E); both as a CI source through primary ozonide formation (OA/LA + $O_3 \rightarrow$ POZ $\rightarrow$ CI) and as CI sink via a termination reaction (CI + OA/LA = AcAHP), as shown Figs. S8-S11. In other words, both OA and LA are crucial reaction partners for CIs. The base model (see *Materials and Methods*), using $k_{AcAHP} = 2.2 \times 10^{-19}$ $cm^{-3} \cdot molecule^{-1} \cdot s^{-1}$ reasonably predicts the decay of OA/LA, while the test model with an elevated k_{AcAHP} (10^{-13} $cm^{-3} \cdot molecule^{-1} \cdot s^{-1}$) predicts decay kinetics that are too fast. Notably, the reported gas-phase value for k_{AcAHP} (10^{-10} $cm^{-3} \cdot molecule^{-1} \cdot s^{-1}$ [23]) is 9 orders of magnitude larger, highlighting the dramatic differences between gas- and condensed-phase reaction rates.

Following independent determinations of k_{AlAHP} and k_{AcAHP} described above, we performed new ozonolysis experiments with OA (or LA) aerosols in the presence of saturated CI scavenger (*i.e.,* $C_{24}OH$) as shown in Figs. 4F-4G. This allows, in a single reactive system, to simultaneously evaluate the magnitude of k_{AlAHP} and k_{AcAHP}. CIs, generated from the ozonolysis of OA (or LA), undergo competitive bimolecular reactions with either the parent acid (OA/LA) forming AcAHPs (k_{AcAHP}) or alternatively with the $C_{24}OH$ scavenger to produce AlAHPs (k_{AlAHP}). Further mechanism

analysis is provided in Figs. S13 and S15. The base model assumes identical condensed-phase rate constants for both k_{AcAHP} and k_{AlAHP} (*i.e.*, 2.2×10^{-19} $cm^{-3} \cdot molecule^{-1} \cdot s^{-1}$), which reproduce the observed decay kinetics of OA, LA, and $C_{24}OH$. In contrast, a test model using a larger rate constant (10^{-13} $cm^{-3} \cdot molecule^{-1} \cdot s^{-1}$) systematically overpredicts the decay rates, particularly for $C_{24}OH$. This is because CIs are the sole sink for $C_{24}OH$, making its kinetics particularly sensitive to the magnitudes of k_{AcAHP} and k_{AlAHP}.

Integrating the ozonolysis kinetic data from Tri, OA, LA, and saturated CI scavengers (HDA, $C_{20}OH$ and $C_{24}OH$), we conclude that the base model, employing substantially slower condensed-phase rates for k_{AlAHP} and k_{AcAHP} (10^{-19} $cm^{-3} \cdot molecule^{-1} \cdot s^{-1}$) consistently explains both the reaction kinetics and the formation of characteristic AlAHPs and AcAHPs products. These condensed-phase rates are approximately seven to ten orders of magnitude smaller than their analogous gas-phase values [23]. Notably, variations in the condensed-phase bimolecular termination rates of CIs directly regulate the CI flux available for unimolecular decomposition to OH radicals, thereby controlling the overall oxidation rate of organic aerosols.

To evaluate whether the observed rate reduction extends to OH initiated oxidation of organic aerosols (thereby isolating OH chemistry from ozonolysis pathways), we conducted a series of measurements using Sqe, Tri, OA, and LA aerosols exposed to OH radicals in a continuous flow stirred tank reactor (CFSTR, see *Materials and Methods*). Figure 5A shows Tri decay kinetics in the presence of $C_{20}OH$. The reaction mechanism shown in Fig. S16 illustrates how OH and O_2 addition to Tri generates β-hydroxyperoxy radicals (β-OH-RO_2•), which subsequently form CIs. Our base model [14], incorporating a substantially slower rate constant ($k_{AlAHP} = 6.7 \times 10^{-19}$ $cm^{-3} \cdot molecule^{-1} \cdot s^{-1}$) reasonably reproduces the kinetic profiles of Tri and $C_{20}OH$ consumption, as well

as AlAHPs formation (Figs. 5A-5B). In contrast, a test model with k_{AlAHP} = 10^{-13} $cm^{-3} \cdot molecule^{-1} \cdot s^{-1}$ predicts complete $C_{20}OH$ consumption by 1500 s, whereas the experimental measurements show that approximately 80% of $C_{24}OH$ remains. As discussed above, this significant discrepancy arises because the CI + $C_{20}OH$ reaction serves as the exclusive sink for $C_{20}OH$ [6], making the kinetics of this scavenger particularly sensitive to the condensed-phase value of k_{AlAHP}.

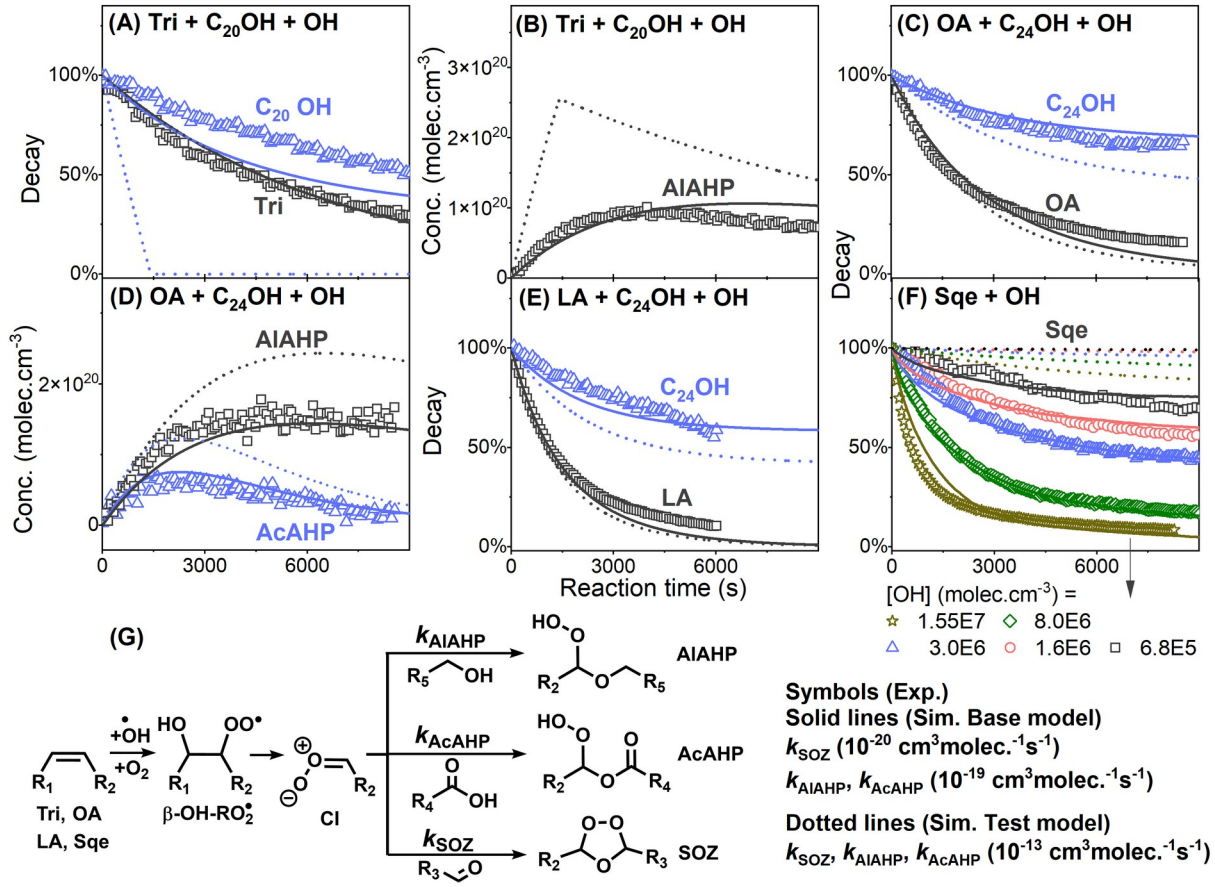

Figure 5. (A-F) Experimental (symbols) and model simulation (lines) results for Tri, $C_{20}OH$, AlAHP, OA, $C_{24}OH$, AcAHP, LA, and Sqe [8] during the OH radical-initiated oxidation of Tri, OA, LA, and Sqe with or without external CI scavenger ($C_{20}OH$ or $C_{24}OH$) in the CFSTR. Solid and dotted lines are simulations from the base model and test model, respectively. For example, panel A illustrates the decay of Tri and $C_{20}OH$ as a function of reaction time for Tri + $C_{20}OH$ mixture aerosols. (G) Reaction scheme showing CI formation from OH initiated reactions of Tri, OA, LA, and Sqe, followed by CI bimolecular reactions with alcohols ($C_{20}OH$ or $C_{24}OH$), carboxylic acids (OA or LA), and aldehydes (e.g., C_{17} CHO, C_{22} CHO, and C_{27} CHO). The experimental product concentrations were scaled to the corresponding simulated values from the Base model.

Furthermore, we investigate the kinetic competition between k_{AlAHP} and k_{AcAHP} during OH initiated oxidation of OA (or LA) aerosols (Figs. 5C-5E) using $C_{24}OH$ as a competitive scavenger. The CIs generated through OH reactions with OA/LA (Figs. S17-S19) undergo competitive bimolecular reactions with either the parent acid (OA or LA) with a rate constant k_{AcAHP} or with $C_{24}OH$ with a rate given by k_{AlAHP}. The base model, setting the rate constants for k_{AlAHP} and k_{AcAHP} to 2.2×10^{-19} $cm^{-3} \cdot molecule^{-1} \cdot s^{-1}$, reasonably reproduces the observed kinetics of OA, LA, $C_{24}OH$, AcAHPs, and AlAHPs. In contrast, the test model, with both k_{AlAHP} and k_{AcAHP} elevated to 10^{-13} $cm^{-3} \cdot molecule^{-1} \cdot s^{-1}$, predicts much faster decay kinetics of OA, LA, and $C_{24}OH$ than is observed in the experiments. Unlike the Tri + $C_{20}OH$ + OH reaction system, complete consumption of $C_{24}OH$ is not observed. This difference arises from competitive CIs depletion pathways in the OA/LA + $C_{24}OH$ + OH systems, where reactions with the parent acids (OA or LA) significantly reduce the $C_{24}OH$ consumption rate when larger k_{AlAHP} and k_{AcAHP} values are used.

The condensed-phase rate constant for CI + aldehyde reactions forming SOZs (k_{SOZ}) has been established to be within range of 10^{-15} - 10^{-20} $cm^{-3} \cdot molecule^{-1} \cdot s^{-1}$ [8, 30, 32-34, 36, 37], whereas representative gas-phase k_{SOZ} values are between 10^{-12} and 10^{-13} $cm^{-3} \cdot molecule^{-1} \cdot s^{-1}$ [20, 23]. To further constrain k_{SOZ}, we analyze published OH initiated oxidation experiments of Sqe aerosols (Fig. 5F) [8], a mechanistically distinct system from Tri (OA or LA) oxidation. Sqe oxidation occurs via OH addition followed by O_2 incorporation to generate β-OH-RO_2• radicals that decompose into CIs and α-hydroxy alkyl radicals (α-OH-R•). Subsequent α-OH-R• reactions produce condensed-phase aldehydes ($C_{27}H_{44}O$, $C_{22}H_{36}O$, and $C_{17}H_{28}O$) [8] that serve as *in-situ* CI scavengers. The base model taken from Ref. [8], employing $k_{SOZ} = 5.5 \times 10^{-20}$ $cm^{-3} \cdot molecule^{-1} \cdot s^{-1}$, reproduces the experimental Sqe decay across OH concentrations ranging from 6.8×10^5 to 1.55×10^7

molecules · cm^{-3}. Conversely, test models using either a gas-phase equivalent k_{SOZ} (10^{-13} cm^{-3} · molecule^{-1} · s^{-1} (Fig. 5F)) or using a condensed phase value (1.66×10^{-15} cm^{-3} · molecule^{-1} · s^{-1}, Fig. S20) proposed by Müller *et al.* [32], underpredict the Sqe reactivity observed experimentally. This discrepancy reflects competing Sqe autoxidation pathways (Fig. 1), *i.e.*, unimolecular CI decomposition regenerates OH radicals to enhance oxidation, while elevated k_{SOZ} shifts the dominant sink to bimolecular CI-aldehyde reactions that suppress OH recycling and decelerate overall oxidation.

This analysis reveals significant derivations in organic aerosol oxidation when assuming gas-phase or diffusion-limited rate coefficients (k_{AcAHP}, k_{AlAHP}, and k_{SOZ}). To quantitatively evaluate these phase-dependent effects, we examine effective reaction probabilities (γ_{eff}) of Tri and Sqe previously reported in Refs. [8, 14, 35]. Figures 6B-6D assess the individual influences of k_{AcAHP}, k_{AlAHP}, and k_{SOZ}, with Figures 6B and 6C characterizing the classic ozonolysis processes where CI-driven OH chemistry appears, while Fig. 6D specifically examines OH initiated oxidation of Sqe in the absence of ozonolysis reactions.

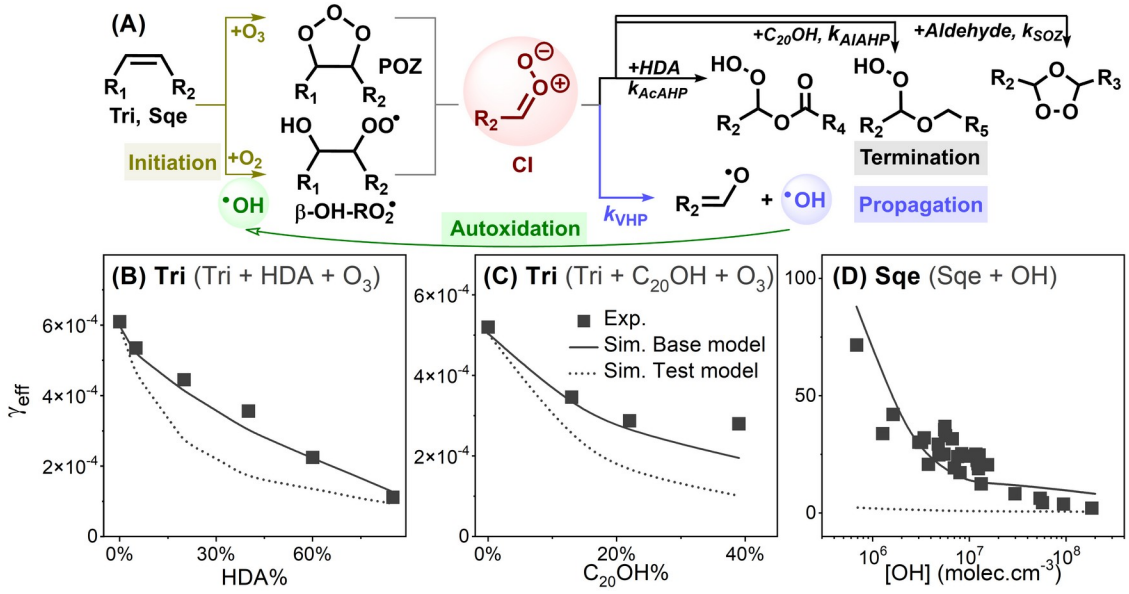

Figure 6. (A) Reaction scheme showing CI formation via O_3/OH initiated reactions of Tri and Sqe, followed by CI bimolecular reactions with HDA, $C_{20}OH$, and aldehydes. The OH regeneration from CI unimolecular decomposition drives the autoxidation chain reaction. (B-C) Experimental (symbols) [14, 35] and simulated (lines) effective reaction probabilities (γ_{eff}) of Tri as a function of CI scavenger (HDA or $C_{20}OH$) concentration in a flowtube reactor. (D) Experimental [8] and simulated effective reaction probabilities (γ_{eff}) of Sqe as a function of [OH] in the CFSTR. Solid and dotted lines represent simulations from the base model (employing k_{AlAHP}, k_{AcAHP}, 10^{-19}; and k_{SOZ}, 10^{-20} $cm^{-3} \cdot molecule^{-1} \cdot s^{-1}$) and test model (using k_{AlAHP}, k_{AcAHP}, and k_{SOZ}, 10^{-13} $cm^{-3} \cdot molecule^{-1} \cdot s^{-1}$), respectively.

Figures 6A and 6B show that both experimental and simulated values of γ_{eff} for Tri decrease with increasing scavenger concentrations (*i.e.*, HDA or $C_{20}OH$). The base model simulations, employing k_{AcAHP} and k_{AlAHP} at values of 10^{-19} $cm^{-3} \cdot molecule^{-1} \cdot s^{-1}$, reproduce the experimental trends. In contrast, test models, implementing larger rate constants (10^{-13} $cm^{-3} \cdot molecule^{-1} \cdot s^{-1}$) exhibit substantial deviations (up to 2-fold) from experimental observations. This systematic discrepancy reveals that gas-phase-derived rate constants [23], when applied to condensed-phase systems, fail to capture the actual bimolecular reactions between CIs and either carboxylic acids (HDA) or alcohols ($C_{20}OH$), thereby highlighting fundamental differences between gas- and condensed-phase reaction dynamics during the ozonolysis of organic aerosols.

Figure 6C shows γ_{eff} for OH-initiated Sqe oxidation [8], revealing an inverse correlation between γ_{eff} and [OH] providing evidence for radical chain cycling (i.e., autoxidation). The chain cycling reaction, shown in Fig. 1, is: Sqe + •OH + O_2 → β-OH-RO_2• → CI (+ α-OH-R•) → •OH explains why $\gamma_{eff} > 1$. This [OH] dependence arises because increased radical concentrations at higher [OH] promotes radical densities that favoring radical + radical termination reactions (e.g., β-OH-RO_2• + β-OH-RO_2•), which do not lead to chain cycling. The α-OH-R• reactions produce C_{27}, C_{22} and C_{17} aldehydes (Fig. S21) that react with CIs to form SOZs (k_{SOZ}). The base model (k_{SOZ}

= 5.5 × 10^{-20} $cm^{-3} \cdot molecule^{-1} \cdot s^{-1}$) reproduces the observed Sqe autoxidation rates (γ_{eff}), whereas the test model using a larger k_{SOZ} (10^{-13} $cm^{-3} \cdot molecule^{-1} \cdot s^{-1}$) yields dramatically lower γ_{eff} values (0.6 to 2.3) across all [OH], which is inconsistent with experimental observations. This discrepancy becomes particularly pronounced at [OH] = 6.8 × 10^5 $molecules \cdot cm^{-3}$, where experiments yield $\gamma_{eff} \approx 70$ (indicating the consumption of at least 70 Sqe molecules per gas-phase OH collision), while the test model predicts $\gamma_{eff} \approx 2.3$, a 30-fold underestimation of the autoxidation rate. These results show that rapid CI-aldehyde termination strongly suppresses autoxidation, particularly under low [OH] conditions where CI unimolecular decomposition would otherwise dominate the oxidation process.

Comparative analyses of the predictions from the base and test models reveal fundamental kinetic differences in atmospheric oxidation pathways of organic aerosols. The OH-initiated Sqe oxidation demonstrates higher sensitivity to variations in CI bimolecular reaction rates, exhibiting up to 30-fold decreases in oxidation rates (Fig. 6C) when implementing larger rates, compared to only 2-fold reactivity reduction in Tri ozonolysis. The divergence arises because Sqe oxidation depends critically on CI unimolecular decomposition pathway to generate OH radicals, whereas Tri oxidation primarily follows ozonolysis pathways. Notably, our constrained condensed-phase rate constants (k_{AcAHP}, k_{AlAHP}, and k_{SOZ}) show less variation (~ 10-fold) than their gas-phase analogs. For instance, the gas-phase rate coefficient of the simplest CI (CH_2OO) with formic acid (k_{AcAHP} = 10^{-10} $cm^{-3} \cdot molecule^{-1} \cdot s^{-1}$ [22]) exceeds those for CI (CH_3CHOO) + methanol (k_{AlAHP}) and CH_2OO + acetaldehyde (k_{SOZ}) (both 10^{-13} $cm^{-3} \cdot molecule^{-1} \cdot s^{-1}$ [20, 51]) by 1000-fold. These phase-dependent differences in CI reaction competition should not only influence the reactivity of unsaturated organics but also control the relative formation abundance of AcAHP, AlAHP, and SOZ products.

The observed dramatic slowdown in CI bimolecular reaction rates suggest substantial solvation effects [35, 37, 52]. However, the slowdown of the condensed phase reaction rates reported here are larger than can be explained by diffusive limitations alone [35]. This might suggest, analogous to the substantial slowdown of gas phase ion-molecule reactions in aqueous systems, that solvation energy of the CI (a zwitterion) may play a substantial role in raising the barrier for bimolecular reaction rates. The lipidic chains of CI scavengers ($C_{20}OH$, $C_{24}OH$, HDA, OA, LA, and aldehydes) could form aliphatic solvent cages around CIs that require additional energy to disrupt before encountering and reacting with a scavenger. This appears not to strongly influence unimolecular CI decomposition reactions that regenerate OH radicals. Additionally, steric hindrance from CI substituents has been shown to induce significant regio- and stereo-selectivity effects in CI-alkene reactions [29]. These effects potentially explain the differences in rates for longer-chain condensed-phase CIs compared to shorter gas-phase CIs, particularly in lipid-rich environments where scavenger mobility is restricted. While these rate constraints are based on experimental and modeling results, further theoretical calculations are required to understand why these condensed-phase CI bimolecular reaction rates are so small.

4. Atmospheric Implications

Here we report evidence that CIs, which form in the heterogeneous reactions of aerosols upon exposure to O_3 or OH radicals, exhibit condensed-phase bimolecular reactions that are substantially slower (approximately by 10^{10}- to 10^{7}-fold) than analogous gas-phase reactions albeit with much smaller molecular weight CIs. Experimental results confirm that CI scavengers (e.g., C_{27} CHO, $C_{20}OH$, $C_{24}OH$, HDA, OA, and LA) effectively quench CIs reactivity via bimolecular reactions, simultaneously modulating the decay kinetics of aerosols and products distribution

(SOZs, AcAHPs, and AlAHPs). Kinetic modeling reveals that that incorporating these slower condensed phase rates (k_{AlAHP}, k_{AcAHP}, 10^{-19} and k_{SOZ}, 10^{-20} $cm^{-3} \cdot molecule^{-1} \cdot s^{-1}$) match observed reaction profiles, whereas the test models assuming faster "gas phase like" or diffusion limited rates (10^{-13} $cm^{-3} \cdot molecule^{-1} \cdot s^{-1}$) significantly overpredict CI reactivity and underpredict heterogeneous oxidation rates. This exact reason for the slowdown of CI bimolecular reactivity in aerosols is currently unclear but could originate from the increased size, complexity, steric hindrance, as well as solvation effects of CI in the condensed phase. Computational approaches using explicit solvent or polarizable continuum models may offer additional insights into the role of the solvent cage in the observed rate suppression.

Mechanistic analyses identify unimolecular CI decomposition (generating OH radicals) as a dominant chain-propagation step, while CI bimolecular reactions serve as chain-termination reactions. For example, assuming an acid concentration of 5×10^{20} $molecule \cdot cm^{-3}$, the gas-phase-like bimolecular rates yield a CI lifetime (τ) of 10^{-5} ms ($\tau \sim 1 / k_{AcAHP,\ AlAHP,\ SOZ}$), which is in contrast to the slowdown of condensed-phase bimolecular rates that extends τ to 10 ms. This allows CI unimolecular decomposition to regenerate OH radicals, which dominate the reaction landscape of organic aerosols. This framework explains why elevated CI bimolecular rates suppress autoxidation by 2-30× lower than experimental effective reaction probabilities, thereby establishing fundamental kinetic constraints on condensed-phase CI bimolecular reactions in organic aging processes. Accurate determination of these rates is consequently essential for understanding the aerosol aging, air quality impacts, and autoxidative destruction of bioorganic molecules.

Associated content

Supporting Information.

Additional experimental details and mechanistic analyses are provided in the Supporting Information. Figures S1-S21 showcase complementary experimental and simulated profiles, along with representative reaction pathways. Tables S1-S5 list the reaction steps and corresponding rate constants employed in the models.

Author information

Corresponding Authors

Meirong Zeng - *College of Smart Energy, Shanghai Jiao Tong University, Shanghai 200240, P.R. China;* orcid.org/0000-0003-3902-7430; Email: meirongzeng@sjtu.edu.cn

Kevin R. Wilson - *Chemical Sciences Division, Lawrence Berkeley National Laboratory, Berkeley, California 94720, United States;* orcid.org/0000-0003-0264-0872; Email: kwilson@lbl.gov

Notes

The authors declare no competing financial interest.

Acknowledgments

M.Z. acknowledges support for the kinetic modeling portion of this work from the National Natural Science Foundation of China (22373066) and Shanghai Science and Technology Innovation Action Plan (24142201500). The experimental measurements were supported by the Gas Phase Chemical Physics program in the Chemical Sciences Geosciences and Biosciences Division of the Office of Basic Energy Sciences of the U.S. Department of Energy under Contract No. DE-AC02-05CH11231. The experimental measurements used the Advanced Light Source,

which is a U.S. Department of Energy Scientific User Facility under contract no. DE-AC02-05CH11231. We thank Bruce Rude for assistance at the ALS.

References

(1) Criegee, R., Mechanism of ozonolysis. *Angew. Chem. Int. Ed.* **1975,** *14* (11), 745−752.

(2) Yang, L.; Zhang, J., Effect of Carbon Chain Length on Nascent Yields of Stabilized Criegee Intermediates in Ozonolysis of a Series of Terminal Alkenes. *J. Am. Chem. Soc.* **2024,** *146* (35), 24591−24601.

(3) Taatjes, C. A., Criegee Intermediates: What Direct Production and Detection Can Teach Us About Reactions of Carbonyl Oxides. *Annu. Rev. Phys. Chem.* **2017,** *68*, 183−207.

(4) Zhang, X.; Barraza, K. M.; Beauchamp, J. L., Cholesterol provides nonsacrificial protection of membrane lipids from chemical damage at air-water interface. *Proc. Natl. Acad. Sci. U.S.A.* **2018,** *115*, 3255–3260.

(5) Zhang, X.; Barraza, K. M.; Upton, K. T.; Beauchamp, J. L., Subtle changes in lipid environment have profound effects on membrane oxidation chemistry. *J. Am. Chem. Soc.* **2018,** *140*, 17492–17498.

(6) Zeng, M.; Heine, N.; Wilson, K. R., Evidence that Criegee intermediates drive autoxidation in unsaturated lipids. *Proc. Natl. Acad. Sci. U. S. A.* **2020,** *117*, 4486–4490.

(7) Zeng, M.; Wilson, K. R., Coupling of Lipid Peroxidation and Criegee Intermediate Mediated Autoxidation in the Heterogeneous Oxidation of Linoleic Acid Aerosols. *Environ. Sci. Technol.* **2025,** *59*, 9178−9187.

(8) Zeng, M.; Wilson, K. R., Evaluating Possible Formation Mechanisms of Criegee Intermediates during the Heterogeneous Autoxidation of Squalene. *Environ. Sci. Technol.* **2024,** *58*, 11587–11595.

(9) Wagner, J. P., Criegee Intermediates in Autoxidation Reactions − Mechanistic Considerations. *J. Phys. Chem. A* **2021,** *125*, 406–410.

(10) Chen, L.; Huang, Y.; Xue, Y.; Jia, Z., Molecular insights into the formation of Criegee intermediates from β-hydroxyperoxy radicals. *Atmos. Environ.* **2024,** *338*, 120828.

(11) Caravan, R. L.; Bannan, T. J.; Winiberg, F. A. F.; Khan, M. A. H.; Rousso, A. C.; Jasper, A. W.; Worrall, S. D.; Bacak, A.; Artaxo, P.; Brito, J.; Priestley, M.; Allan, J. D.; Coe, H.; Ju, Y.; Osborn, D. L.; Hansen, N.; Klippenstein, S. J.; Shallcross, D. E.; Taatjes, C. A.; Percival, C. J., Observational evidence for Criegee intermediate oligomerization reactions relevant to aerosol formation in the troposphere. *Nat. Geosci.* **2024,** *17* (3), 219−226.

(12) Vereecken, L.; Novelli, A.; Taraborrelli, D., Unimolecular decay strongly limits the atmospheric impact of Criegee intermediates. *Phys. Chem. Chem. Phys.* **2017,** *19*, 31599–31612.

(13) Liu, T.; Elliott, S. N.; Zou, M.; Vansco, M. F.; Sojdak, C. A.; Markus, C. R.; Almeida, R.; Au, K.; Sheps, L.; Osborn, D. L.; Winiberg, F. A. F.; Percival, C. J.; Taatjes, C. A.; Caravan, R. L.; Klippenstein, S. J.; Lester, M. I., OH Roaming and Beyond in the Unimolecular Decay of the Methyl-Ethyl-Substituted Criegee Intermediate: Observations and Predictions. *J. Am. Chem. Soc.* **2023,** *145* (35), 19405−19420.

(14) Zeng, M.; Wilson, K. R., Efficient Coupling of Reaction Pathways of Criegee Intermediates and Free Radicals in the Heterogeneous Ozonolysis of Alkenes. *J. Phys. Chem. Lett.* **2020,** *11*, 6580–6585.

(15) Kroll, J. H.; Smith, J. D.; Che, D. L.; Kessler, S. H.; Worsnop, D. R.; Wilson, K. R., Measurement of fragmentation and functionalization pathways in the heterogeneous oxidation of oxidized organic aerosol. *Phys. Chem. Chem. Phys.* **2009,** *11* (36), 8005–8014.

(16) Fang, Y.; Liu, F.; Barber, V. P.; Klippenstein, S. J.; McCoy, A. B.; Lester, M. I., Deep tunneling in the unimolecular decay of CH_3CHOO Criegee intermediates to OH radical products. *J. Chem. Phys.* **2016,** *145* (23), 234308.

(17) Liu, F.; Beames, J. M.; Petit, A. S.; McCoy, A. B.; Lester, M. I., Infrared-driven unimolecular reaction of CH_3CHOO Criegee intermediates to OH radical products. *Science* **2014,** *345* (6204), 1596−1598.

(18) Taatjes, C. A.; Welz, O.; Eskola, A. J.; Savee, J. D.; Scheer, A. M.; Shallcross, D. E.; Rotavera, B.; Lee, E. P. F.; Dyke, J. M.; Mok, D. K. W.; Osborn, D. L.; Percival, C. J., Direct measurements of conformer-dependent reactivity of the Criegee intermediate CH_3CHOO. *Science* **2013,** *340*, 177−180.

(19) Welz, O.; Savee, J. D.; Osborn, D. L.; Vasu, S. S.; Percival, C. J.; Shallcross, D. E.; Taatjes, C. A., Direct kinetic measurements of Criegee intermediate (CH_2OO) formed by reaction of CH_2I with O_2. *Science* **2012,** *335*, 204−207.

(20) Taatjes, C. A.; Welz, O.; Eskola, A. J.; Savee, J. D.; Osborn, D. L.; Lee, E. P.; Dyke, J. M.; Mok, D. W.; Shallcross, D. E.; Percival, C. J., Direct measurement of Criegee intermediate (CH_2OO) reactions with acetone, acetaldehyde, and hexafluoroacetone. *Phys. Chem. Chem. Phys.* **2012,** *14* (30), 10391−10400.

(21) Chao, W.; Lin, Y. H.; Yin, C.; Lin, W. H.; Takahashi, K.; Lin, J. J., Temperature and isotope effects in the reaction of CH_3CHOO with methanol. *Phys. Chem. Chem. Phys.* **2019,** *21* (25), 13633−13640.

(22) Welz, O.; Eskola, A. J.; Sheps, L.; Rotavera, B.; Savee, J. D.; Scheer, A. M.; Osborn, D. L.; Lowe, D.; Murray Booth, A.; Xiao, P.; Anwar, H. K. M.; Percival, C. J.; Shallcross, D. E.;

Taatjes, C. A., Rate coefficients of C1 and C2 Criegee intermediate reactions with formic and acetic Acid near the collision limit: direct kinetics measurements and atmospheric implications. *Angew. Chem. Int. Ed. Engl.* **2014,** *53*, 4547–4550.

(23) Khan, M. A. H.; Percival, C. J.; Caravan, R. L.; Taatjes, C. A.; Shallcross, D. E., Criegee intermediates and their impacts on the troposphere. *Environ. Sci. Proc. Impacts* **2018,** *20* (3), 437–453.

(24) Tobias, H. J.; Ziemann, P. J., Kinetics of the Gas-Phase Reactions of Alcohols, Aldehydes, Carboxylic Acids, and Water with the C13 Stabilized Criegee Intermediate Formed from Ozonolysis of 1-Tetradecene. *J. Phys. Chem. A* **2001,** *105*, 6129-6135.

(25) Wang, P.; Wang, Y.; Wang, J.; Mellouki, A.; Daële, V.; Ren, Y.; McGillen, M. R., Development of a Relative Rate Technique to Measure Criegee Intermediate Reactivity. *Environ. Sci. Technol. Lett.* **2025,** *12* (7), 842–847.

(26) Debnath, A.; Rajakumar, B., Experimental and theoretical study of Criegee intermediate (CH_2OO) reactions with *n*-butyraldehyde and isobutyraldehyde: kinetics, implications and atmospheric fate. *Phys. Chem. Chem. Phys.* **2024,** *26* (8), 6872–6884.

(27) Chhantyal-Pun, R.; Rotavera, B.; McGillen, M. R.; Khan, M. A. H.; Eskola, A. J.; Caravan, R. L.; Blacker, L.; Tew, D. P.; Osborn, D. L.; Percival, C. J.; Taatjes, C. A.; Shallcross, D. E.; Orr-Ewing, A. J., Criegee Intermediate Reactions with Carboxylic Acids: A Potential Source of Secondary Organic Aerosol in the Atmosphere. *ACS Earth Space Chem.* **2018,** *2*, 833–842.

(28) Watson, N. I.; Black, J. A.; Stonelake, T. M.; Knowles, P. J.; Beames, J. M., An extended computational study of Criegee intermediate - alcohol reactions. *J. Phys. Chem. A* **2019,** *123*, 218–229.

(29) Enami, S.; Colussi, A. J., Efficient scavenging of Criegee intermediates on water by surface-active cis-pinonic acid. *Phys. Chem. Chem. Phys.* **2017,** *19* (26), 17044–17051.

(30) Gallimore, P. J.; Griffiths, P. T.; Pope, F. D.; Reid, J. P.; Kalberer, M., Comprehensive modeling study of ozonolysis of oleic acid aerosol based on real-time, online measurements of aerosol composition. *J. Geophys. Res. Atmos.* **2017,** *122* (8), 4364–4377.

(31) Berkemeier, T.; Mishra, A.; Mattei, C.; Huisman, A. J.; Krieger, U. K.; Pöschl, U., Ozonolysis of Oleic Acid Aerosol Revisited: Multiphase Chemical Kinetics and Reaction Mechanisms. *ACS Earth Space Chem.* **2021,** *5* (12), 3313–3323.

(32) Müller, M.; Mishra, A.; Berkemeier, T.; Hausammann, E.; Peter, T.; Krieger, U. K., Electrodynamic balance–mass spectrometry reveals impact of oxidant concentration on product composition in the ozonolysis of oleic acid. *Phys. Chem. Chem. Phys.* **2022,** *24* (44), 27086–27104.

(33) Zhou, Z.; Lakey, P. S. J.; von Domaros, M.; Wise, N.; Tobias, D. J.; Shiraiwa, M.; Abbatt, J. P. D., Multiphase Ozonolysis of Oleic Acid-Based Lipids: Quantitation of Major Products and Kinetic Multilayer Modeling. *Environ. Sci. Technol.* **2022,** *56* (12), 7716−7728.

(34) Lakey, P. S. J.; Zuend, A.; Morrison, G. C.; Berkemeier, T.; Wilson, J.; Arata, C.; Goldstein, A. H.; Wilson, K. R.; Wang, N.; Williams, J.; Abbatt, J. P. D.; Shiraiwa, M., Quantifying the impact of relative humidity on human exposure to gas phase squalene ozonolysis products. *Environ. Sci.: Atmos.* **2023,** *3* (1), 49−64.

(35) Reynolds, R.; Ahmed, M.; Wilson, K. R., Constraining the Reaction Rate of Criegee Intermediates with Carboxylic Acids during the Multiphase Ozonolysis of Aerosolized Alkenes. *ACS Earth Space Chem.* **2023,** *7*, 901–911.

(36) Willis, M. D.; Wilson, K. R., Coupled Interfacial and Bulk Kinetics Govern the Timescales of Multiphase Ozonolysis Reactions. *J. Phys. Chem. A* **2022,** *126* (30), 4991−5010.

(37) Heine, N.; Houle, F. A.; Wilson, K. R., Connecting the elementary reaction pathways of Criegee intermediates to the chemical erosion of squalene interfaces during ozonolysis. *Environ. Sci. Technol.* **2017,** *51*, 13740–13748.

(38) Wilson, K. R.; Peterka, D. S.; Jimenez-Cruz, M.; Leone, S. R.; Ahmed, M., VUV photoelectron imaging of biological nanoparticles: ionization energy determination of nanophase glycine and phenylalanine-glycine-glycine. *Phys. Chem. Chem. Phys.* **2006,** *8* (16), 1884−1890.

(39) Wilson, K. R.; Jimenez-Cruz, M.; Nicolas, C.; Belau, L.; Leone, S. R.; Ahmed, M., Thermal vaporization of biological nanoparticles: fragment-free vacuum ultraviolet photoionization mass spectra of tryptophan, phenylalanine-glycine-glycine, and β-carotene. *J. Phys. Chem. A* **2006,** *110*, 2106–2113.

(40) Reynolds, R. S.; Wilson, K. R., Unraveling the Meaning of Effective Uptake Coefficients in Multiphase and Aerosol Chemistry. *Acc. Chem. Res.* **2025,** *58* (3), 366–374.

(41) Houle, F. A.; Wiegel, A. A.; Wilson, K. R., Changes in reactivity as chemistry becomes confined to an interface. The case of free radical oxidation of $C_{30}H_{62}$ alkane by OH. *J. Phys. Chem. Lett.* **2018,** *9*, 1053–1057.

(42) Houle, F. A.; Hinsberg, W. D.; Wilson, K. R., Oxidation of a model alkane aerosol by OH radical: the emergent nature of reactive uptake. *Phys. Chem. Chem. Phys.* **2015,** *17* (6), 4412−4423.

(43) Wolfram Research, Inc., Mathematica, Champaign, Illinois, Version 13.0.0 ed., 2021.

(44) Che, D. L.; Smith, J. D.; Leone, S. R.; Ahmed, M.; Wilson, K. R., Quantifying the reactive uptake of OH by organic aerosols in a continuous flow stirred tank reactor. *Phys. Chem. Chem. Phys.* **2009,** *11*, 7885–7895.

(45) Wiegel, A. A.; Liu, M. J.; Hinsberg, W. D.; Wilson, K. R.; Houle, F. A., Diffusive confinement of free radical intermediates in the OH radical oxidation of semisolid aerosols. *Phys. Chem. Chem. Phys.* **2017,** *19* (9), 6814–6830.

(46) Liu, M. J.; Wiegel, A. A.; Wilson, K. R.; Houle, F. A., Aerosol Fragmentation Driven by Coupling of Acid-Base and Free-Radical Chemistry in the Heterogeneous Oxidation of Aqueous Citric Acid by OH Radicals. *J. Phys. Chem. A* **2017,** *121*, 5856–5870.

(47) Wiegel, A. A.; Wilson, K. R.; Hinsberg, W. D.; Houle, F. A., Stochastic methods for aerosol chemistry: a compact molecular description of functionalization and fragmentation in the heterogeneous oxidation of squalane aerosol by OH radicals. *Phys. Chem. Chem. Phys.* **2015,** *17*, 4398–4411.

(48) Nicolaides, N., Skin lipids: their biochemical uniqueness. *Science* **1974,** *186*, 19–26.

(49) Mao, C.; Xiao, P.; Tao, X. N.; Qin, J.; He, Q. T.; Zhang, C.; Guo, S. C.; Du, Y. Q.; Chen, L. N.; Shen, D. D.; Yang, Z. S.; Zhang, H. Q.; Huang, S. M.; He, Y. H.; Cheng, J.; Zhong, Y. N.; Shang, P.; Chen, J.; Zhang, D. L.; Wang, Q. L.; Liu, M. X.; Li, G. Y.; Guo, Y.; Xu, H. E.; Wang, C.; Zhang, C.; Feng, S.; Yu, X.; Zhang, Y.; Sun, J. P., Unsaturated bond recognition leads to biased signal in a fatty acid receptor. *Science* **2023,** *380* (6640), eadd6220.

(50) Yin, H.; Xu, L.; Porter, N. A., Free radical lipid peroxidation: mechanisms and analysis. *Chem. Rev.* **2011,** *111* (10), 5944–5972.

(51) McGillen, M. R.; Curchod, B. F. E.; Chhantyal-Pun, R.; Beames, J. M.; Watson, N.; Khan, M. A. H.; McMahon, L.; Shallcross, D. E.; Orr-Ewing, A. J., Criegee intermediate–alcohol reactions, a potential source of functionalized hydroperoxides in the atmosphere. *ACS Earth Space Chem.* **2017,** *1* (10), 664–672.

(52) Pryor, W. A.; Smith, K., The Viscosity Dependence of Bond Homolysis. A Qualitative and Semiquantitative Test for Cage Return. *J. Am. Chem. Soc.* **1970,** *92*, 5403–5412.

Table of Contents Graphic